FSI-08-TN78

The Non-Condensable Gas Model in FLOW-3D® [1]

James Brethour
Flow Science, Inc., Santa Fe, NM USA 87505

Overview

The non-condensable gas model is built upon the two-fluid, liquid/vapor phase change model and includes the effects of a non-condensable gas present in the vapor space. The new model is designed to work only with the two-fluid phase change model because the spatial distribution of vapor and gas components is needed to predict the phase change behavior. By contrast, the one-fluid phase change model assumes spatially uniform pressure and temperature throughout the gas phase. The assumption of a uniform gas/vapor concentration in a two-component gas would rarely be valid. This model is the basis of work completed to simulate the ullage space of cryogenic tanks[2], but it is applicable to any two-component gas problem.

What was added to the liquid/vapor two-fluid phase change model?

The liquid/vapor two-fluid phase change model assumes that gas phase regions are:

1) composed entirely of the vapor of the liquid phase and could therefore condense completely into the liquid phase
2) the total gas pressure always tries to equilibrate to the saturation pressure of the liquid.

Addition of non-condensable gas requires:

1) the solution for an additional transported quantity that tracks the concentration of the non-condensable gas,
2) modifications to the pressure iteration schemes to account for a non-uniform gas constant,
3) changes to the energy equation due to a non-uniform heat capacity,
4) alterations to the phase change routine to account for the partial pressure of the vapor (which is the total gas pressure in the liquid/vapor model).

The model does not account for variations of viscosity or thermal conductivity of the gas phase because changes of these properties are considered insignificant for most vapor-gas systems.

Assumptions

The new model assumes that the vapor-gas mixtures can mix in any proportion. The ideal gas assumption holds for all temperatures and pressures encountered in the vapor-gas

phase (as is used for all gas regions in ***FLOW-3D***). Because typically the flow dynamics cannot be predicted at the small scales at the gas-liquid, the phase change mass flux is approximated as a linear function of the difference between the saturation pressure of the vapor and its local partial pressure. The proportionality constant contains an *accommodation coefficient* and is also a function of temperature – higher temperatures slow mass transfer because of the greater distance between gas molecules.

Quantification of the non-condensable gas component

The goal of this work is to include the effect of a non-condensable gas within a gas/vapor region. In order to add the effects of a non-condensable component, an additional quantity (which is transported with the gas flow) must be computed to represent the amount of non-condensable gas present. The quantity chosen is ρ_{nc}, which represents the *microscopic density* of non-condensable gas within each computational cell. Because it is a microscopic quantity, the value of ρ_{nc} does *not* vary due to the available volume in each cell. The resulting transport equation for ρ_{nc} is:

$$\frac{\partial \rho_{nc}}{\partial t} + \nabla \cdot \left(\rho_{nc} \mathbf{v} \right) = D_{nc} \nabla^2 \rho_{nc} \,. \tag{1}$$

Here $\mathbf{v}$ is the local fluid velocity and D_{nc} is the diffusion coefficient of the non-condensable gas within the vapor mixture. Note that this equation (and others in this note) is simplified as it does not include ***FLOW-3D***'s VOF and FAVOR^{TM} functions. Because the non-condensable component does not evaporate or condense, the total quantity within the vapor bubble is constant unless there is a source or sink present or there is flow from an adjacent mesh boundary.

Details of the model

In the liquid/vapor two-fluid phase change model[3], the mass transfer rate is computed based on the difference between the local saturation pressure of the liquid, P_{liq}^{sat}, and the vapor pressure. With the addition of the non-condensable gas, the partial pressure of the vapor, P_{vap}, is used to compute the mass transfer rate at fluid interfaces:

$$\text{Mass transfer rate} = C \sqrt{\frac{1}{2\pi R_{vap} T}} \left(P_{liq}^{sat} - P_{vap} \right). \tag{2}$$

Here C is the *accommodation coefficient* (called *rsize* in the ***FLOW-3D*** input file), R_{vap} is the gas constant of the vapor, T is the local temperature, P_{vap} is the local vapor pressure, and P_{liq}^{sat} is the saturation pressure of the liquid corresponding to the local temperature, derived from the Clausius-Clapeyron equation[4]:

$$P_{liq}^{sat} = P_c \exp\left[-\frac{1}{T_{EXP}} \left(\frac{1}{T} - \frac{1}{T_c} \right) \right]. \tag{3}$$

Here (P_c, T_c) is a point on the saturation curve and T_{EXP} is a fitting parameter, typically equal to

$$T_{EXP} = \frac{(\gamma - 1)c_v^{vap}}{\Delta H_v}, \tag{4}$$

where γ is the ratio of the heat capacity of the vapor at constant pressure to its heat capacity at constant volume (c_v^{vap}), and ΔH_v is its latent heat of vaporization.

P_{vap} in Equation (2) is computed based on the vapor density within the computational cell. First, we need to compute the gas density in the computational cell. In ***FLOW-3D***, we store the macroscopic density of the fluid mixture, ρ (i.e., the average density of all fluid components in the cell). We know if the density of the liquid phase is ρ_{liq}, then the density of the gas mixture in the remainder of the cell (if there is gas phase in the cell) is:

$$\rho_g = \frac{\rho - f\rho_{liq}}{1 - f}. \tag{5}$$

Here f is the updated volume fraction of liquid in the cell. Note that Equation (5) is valid only for values of f<1; cells that contain no gaseous phase are not considered in the phase change model. The total gas density is the sum of the vapor and non-condensable gas densities:

$$\rho_g = \rho_{vap} + \rho_{nc} \tag{6}$$

where ρ_{vap} is the density of the vapor portion of the gas phase. The vapor pressure in the gas phase is then computed from the ideal gas law:

$$P_{vap} = \rho_{vap} R_{vap} T. \tag{7}$$

Likewise, the partial pressure of the non-condensable gas is

$$P_{nc} = \rho_{nc} R_{nc} T \tag{8}$$

where R_{nc} is the gas constant of the non-condensable gas. Also, by the definition of partial pressures for a two-component system,

$$P = P_{vap} + P_{nc}. \tag{9}$$

Solving Equations (6) to (9) yields the microscopic densities and partial pressures of the two gas components.

It is important to distinguish between microscopic and macroscopic densities. The *microscopic* density is a quantity that represents the actual physical density of the gas or liquid, regardless of the volume of the computational cell. In contrast, the *macroscopic* density represents the quantity of material if it were to be spread out over the entire open volume of the computational cell. Therefore, for cells away from the liquid-gas interface, the microscopic and macroscopic densities are one and the same. At the liquid-gas interface, the relationships between micro and macroscopic densities are

$$\breve{\rho}_g = (1-f)\rho_g \qquad \breve{\rho}_{liq} = f\rho_{liq}\,. \tag{10}$$

where $\breve{\rho}_{liq}$ is the macroscopic liquid density, $\breve{\rho}_g$ is the macroscopic gas density and f is the volume fraction of the computational cell occupied by liquid.

During the solution of the compressible flow, the gas density ρ_g is computed from the differential form:

$$\frac{\partial \rho_g}{\partial t} + \rho_g(\nabla \cdot \mathbf{v}) + \mathbf{v} \cdot \nabla \rho_g = 0\,. \tag{11}$$

However, to ensure a stable numerical coupling between velocities and pressures during the computation, especially in the limit of incompressibility, it is sufficient to use a simpler approximation when evaluating the time-advanced velocities:

$$\frac{\partial \rho_g}{\partial t} + \rho_g(\nabla \cdot \mathbf{v}) = 0\,. \tag{12}$$

During the iterative numerical solution of Equation (12), the pressure and velocity components in every computational cell are updated until Equation (12) is satisfied to a specified convergence criterion. The gas density ρ_g is treated as a function of pressure, with the first term of Equation (11) approximated by

$$\frac{\partial \rho_g}{\partial t} \approx \frac{\rho_g(P^i, T^n) - \rho_g^n}{\Delta t} \tag{13}$$

where, by the ideal gas law

$$\rho_g(P^i, T^n) = \frac{P^i}{\overline{R} T^n} \tag{14}$$

and P^i is the locally computed pressure at the i^{th} *iteration*, $\overline{R}$ is the mean gas constant of the vapor-gas mixture, and T^n is the local temperature computed during the previous *computational cycle*.

The value $\overline{R}$ in Equation (14) depends on the relative concentrations of the vapor and non-condensable gas. The values of both ρ_{nc} and ρ_g are taken from the previous computational cycle and, therefore, are known, and ρ_{vap} is calculated from Equations (6-9). Then $\overline{R}$ is computed as:

$$\overline{R} = \frac{\rho_{vap} R_{vap} + \rho_{nc} R_{nc}}{\rho_g^n}, \tag{14}$$

where ρ_g^n is the gas mixture density computed during the previous computational cycle. At this point, the total pressure P has been computed from the iterative solution to Equations (12) through (14). Upon convergence, a more accurate value of ρ_g is obtained from Equation (11). This represents the gas mixture density in a computational cell.

Now, in a separate step, we compute the temperature of the gas mixture including the phase change; this is also calculated iteratively because of the sensitivity of the condensation/evaporation rate to the local temperature and pressure of the gas-liquid mixture. The liquid-gas mixture temperature T is updated within each iteration. The goal is to predict the change in temperature due to phase change, which is

$$\Delta T_j = \frac{\left(\breve{\rho}_{liq}^j - f\rho_{liq}\right)\Delta H_v}{(1-f)[\rho_{vap} c_v^{vap} + \rho_{nc} c_v^{nc}] + f\rho_{liq} c_v^{liq}}. \tag{15}$$

Here f is the liquid fraction within the computational cell, ρ_{liq} is the microscopic liquid density at the start of the iterations (a constant), and $\breve{\rho}_{liq}^j$ is the updated macroscopic liquid density at iteration j, computed to account for the changing amount of liquid present in the computational cell. As evaporation or condensation occurs, $\breve{\rho}_{liq}^j$ goes down or up, respectively, and the rate of this change is computed by Equation (2). Equations (2) through (8) are computed iteratively until a converged value of $\breve{\rho}_{liq}^j$ is reached (i.e., the change from one iteration to the next is below $10^{-6}*\rho_{liq}$).

Additionally, the calculation of the temperature from thermal energy is affected by the non-condensable component; the effective heat capacity of the gas mixture is

$$\left(\rho c_v\right)^{eff} = f\rho_{liq} + (1-f)\left[\rho_{vap} c_v^{vap} + \rho_{nc} c_v^{nc}\right]. \tag{19}$$

Test problem

The test problem is a simple enclosure containing water, steam and air, whose walls are all adiabatic (no heat or mass flux) except for the bottom, in which a heating element is embedded. Figure 1 shows the computational domain. It is solved as a two-dimensional

problem, with only one cell into the page, and 45 cells in each of the other two directions (totaling 2025 computational cells). The simulation was run for a total of 1800 *s*: 1800*s*. During the first 600 *s*, the heater output is maintained constant at 1,000 *W/m*, thereafter, the heater is shut off. The initial temperature of the entire system is 323 *K* (50°*C*), the initial pressure is 1 *atm*, and the initial volume fraction of the non-condensable gas is 0.8847, which corresponds to a vapor pressure of 11.68 *kPa*, or 100% relative humidity. The physical properties used for the fluids are shown in Table 1.

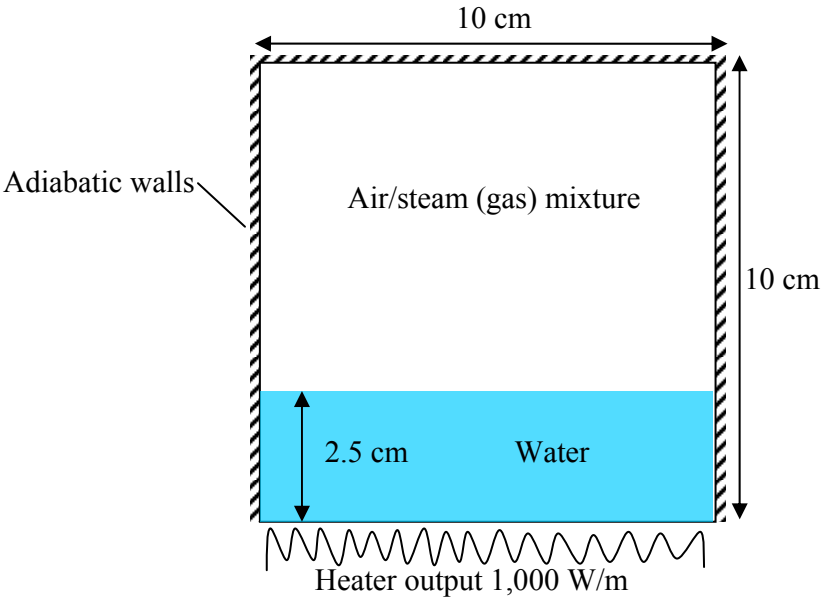

Figure 1: Test problem setup: a two-dimensional container with a heat source.

Heat capacity, water	4182.0	*J/(kg·K)*
Heat capacity, steam	2030.0	*J/(kg·K)*
Heat capacity, air	718.0	*J/(kg·K)*
Heat of vaporization	2260.0	*kJ/kg*
Gas constant, steam	461.5	*J/(kg·K)*
Gas constant, air	286.69	*J/(kg·K)*
Density, water	1000.0	kg/m^3
Thermal expansion coefficient, water	0.0018	K^{-1}
Viscosity of water	1.0	*mPa·s*
Viscosity of steam/air mixture	0.1781	*mPa·s*
P_c	1.013×10^5	*Pa*
T_c	373.0	*K*
T_{EXP}	1.92×10^{-4}	K^{-1}
Accommodation coefficient	1.0	

Table 1: Material property data used in the simulation.

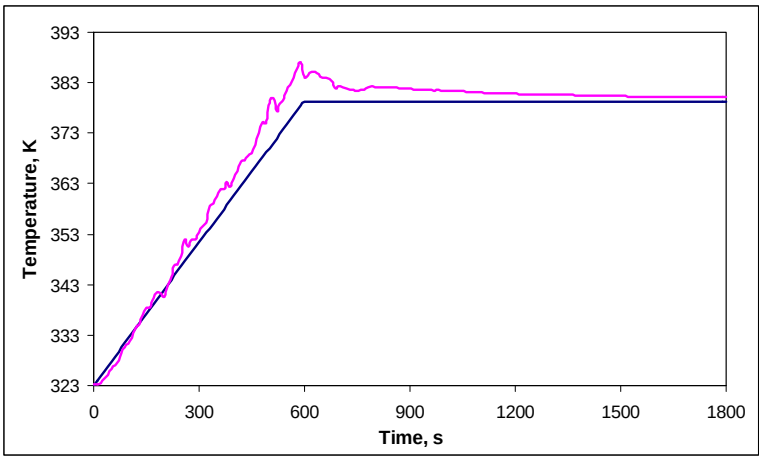

Figure 2: Plot of temperature versus time, showing a comparison of the ***FLOW-3D*** simulation result in the domain center (purple line) and the result from an analytical calculation, based on the assumption of equilibrium throughout the container.

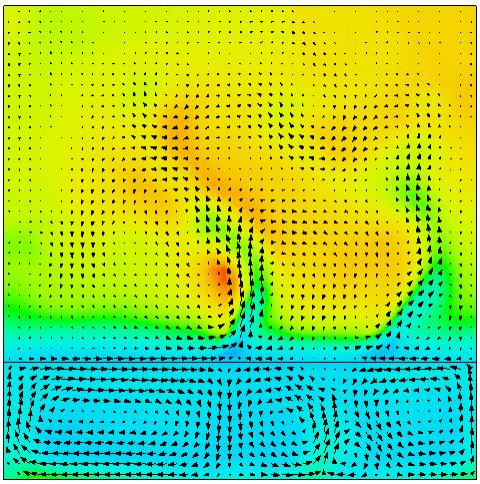

Figure 3: Temperature profile in the domain at t=600 *s*, the moment when the heating element is shut off. The temperature variations in the gas phase are due to natural convection caused by the differing density between steam and air.

Figure 2 shows simulation results for the temperature in the gas phase at the center of the container. The analytical result shown is based on a computational assumption of equilibrium at all times during the simulation, i.e., the water temperature is taken to be uniform and the gas region is in equilibrium with the water. Therefore, the vapor pressure of steam in the gas region is always equal to the saturation pressure of water at the current temperature. Note that the temperature locally does deviate from the equilibrium result: this is to be expected as the system is not truly at equilibrium during the heating phase and only approaches equilibrium after long times of no heat input. What is also interesting is that the gas temperature, although initially below the equilibrium value, rises above it due to compression heating as gas pressure rises with temperature. Figure 3 shows a snapshot of the temperature profile in the container at 600 *s* (exactly when the

heating element is shut off). The oscillations in the temperature seen in Figure 2 are due to the physical instabilities in an inversely stratified medium that develop when lower density gas exists below heavier gas.

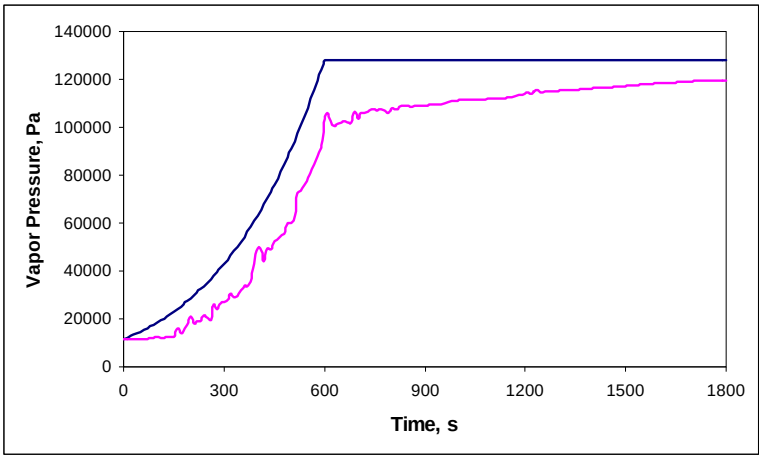

Figure 4: Plot of vapor pressure versus time, showing a comparison of the ***FLOW-3D*** simulation result in the domain center (purple line) and the result from an analytical calculation, based on the assumption of equilibrium throughout the container.

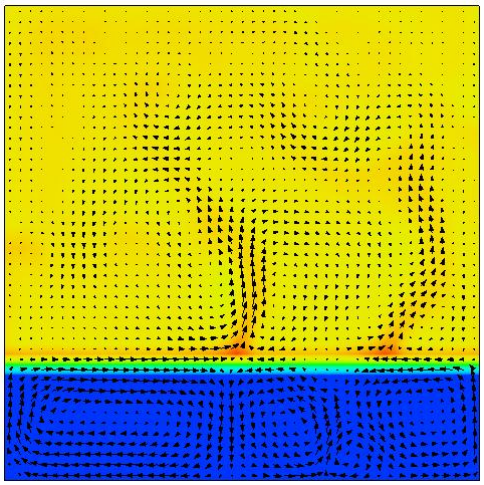

Figure 5: Vapor pressure profile in the domain at t=600 *s*, the moment when the heating element is shut off. Note that the steam rises non-uniformly in the gas phase because steam is less dense than air, even when it is cooler.

Figure 4 shows the vapor pressure as a function of time, again at the center of the container. The ***FLOW-3D*** simulation result fluctuates due to the uneven natural convection of the vapor and remains below the analytical result. This is expected: just as with a physical system, the model is always trying to catch up to the equilibrium result, which is the difference between the actual conditions and the equilibrium condition that drives the evaporation. Thus, during the heating phase, one would always expect to see the vapor pressure lag behind the equilibrium value. Conversely, if an experiment was

performed where cooling is occurring, the vapor pressure curve would always lie above the equilibrium result. At long times after the heating element is shut off, the vapor pressure does approach the equilibrium. Figure 5 shows the spatial distribution of vapor pressure at t=600 *s*.

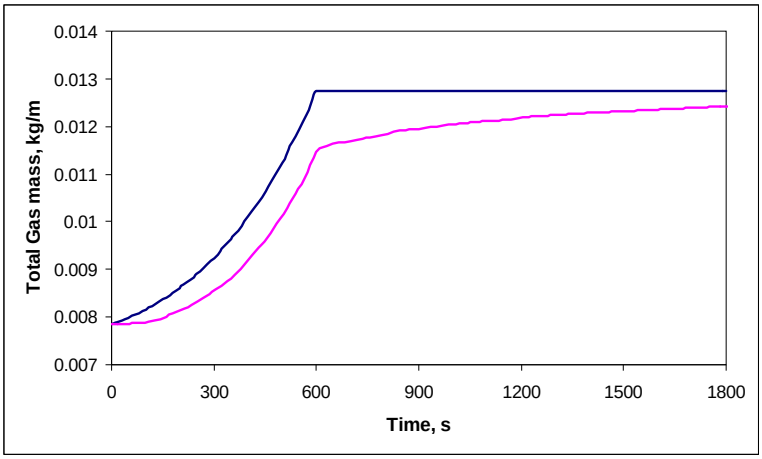

Figure 6: Plot of total gas mass versus time, showing a comparison of the ***FLOW-3D*** simulation result in the domain center (purple line) and the result from an analytical calculation, based on the assumption of equilibrium throughout the container.

Figure 6 shows the expected and simulated total mass of vapor in the container over time. This profile is very similar to that of Figure 4 except the result is much smoother because it is an integral quantity over the entire volume of the container. Again, as expected, the simulated result lags behind the analytical result, with the difference between the two curves the controlling the rate of evaporation. At long times, the equilibrium is approached and the evaporation rate asymptotes to zero.

Remarks

The non-condensable gas model is a powerful addition to ***FLOW-3D*** and enhances the breadth of multiphase problems that can be tackled. The combination of ***FLOW-3D***'s Volume-of-Fluid (VOF), Fractional Area and Volume Representation (FAVOR™) and phase change models give ***FLOW-3D*** users unparalleled computational abilities to simulate highly dynamic gas/liquid multiphase systems.

---

[1] ***FLOW-3D*** is a registered trademark in the USA and other countries.

[2] Gary Grayson, Alfredo Lopez, Frank Chandler, Leon Hastings, Ali Hedayat, and James Brethour, *CFD Modeling of Helium Pressurant Effects on Cryogenic Tank Pressure Rise Rates in Normal Gravity*, 43rd AIAA/ASME/SAE/ASEE Joint Propulsion Conference and Exhibit, 2007.

[3] Hirt, C.W., *Modeling Phase Change and Homogenous Bubbles*, Flow Science Technical Note (FSI-01-TN57), 2001.

[4] Smith, J.M. & H.C. Van Ness, *Introduction to Chemical Engineering Thermodynamics*, 4th Edition, McGraw-Hill, New York, 1987.